Complementary relationship estimation of actual evapotranspiration in extreme cold and arid areas: a case study of the Hotan River Basin, northwest China

Xiaolong Zhang, Bing Shen, Lingmei Huang, Changsen Zhao, Jiqiang Lyu and Quan Quan

ABSTRACT

Application of complementary relationship (CR) approaches using only routine meteorological data is a very convenient method of estimating actual evapotranspiration (ET_a). Reanalysis datasets and remote sensing data provide good tools to overcome the difficulties in obtaining observation data. This study of the Hotan River Basin (HRB) in northwest China serves as a prime example for estimation of ET_a during 2006–2014 by using the modified generalized CR. Based on comparison and analysis, the maximum potential evaporation calculated by the Penman-based equation was adopted. The estimated ET_a rates were verified using a regional water balance method at annual time scales because of the limited available data. The calibration parameter σ was calibrated based on the elevation and underlying surface types. The mean annual ET_a ranged from 2.3 mm to 800 mm during 2006–2014. ET_a rates in the plains regions were higher than those in the mountainous regions. Most of ET_a was concentrated in the months of May to September. A water deficit occurred in the middle and lower regions, while a water surplus occurred in the upper regions. This study not only provided a new concept for calibration, but also a potential solution for different underlying surfaces and time scales.

Key words | complementary relationship, evapotranspiration, extreme cold and arid areas, northwest China, water budget

Xiaolong Zhang
Bing Shen (corresponding author)
Lingmei Huang
Quan Quan
State Key Laboratory Base of Eco-hydraulic Engineering in Arid Area,
Xi'an University of Technology,
Xi'an 710048,
China
E-mail: *shenbing@xaut.edu.cn*

Changsen Zhao
State Key Laboratory of Remote Sensing Science,
Jointly Sponsored by Beijing Normal University and the Institute of Remote Sensing Applications of Chinese Academy of Sciences,
Beijing Normal University,
Beijing 100875,
China

Jiqiang Lyu
School of Environmental Science and Engineering,
Chang'an University,
Xi'an 710054,
China

INTRODUCTION

Actual evapotranspiration (ET_a) is a key variable in the energy, water, and carbon cycles of terrestrial ecosystems (Vinukollu *et al.* 2011; Ma *et al.* 2015a; Crago *et al.* 2016; Aminzadeh & Or 2017; Szilagyi *et al.* 2017). Accurate estimates of ET_a are needed to address a wide range of problems such as global climate change, water balance computation, agricultural management, and hydrological modeling (Xu & Singh 2005; Crago *et al.* 2016). Evapotranspiration is the major water consumption pathway in the water budget, accounting for more than 60% of annual precipitation on a global scale (Oki & Kanae 2006) and more than 90% in extreme arid areas (Glenn *et al.* 2007). ET_a exhibits strong heterogeneity because of the wide spatial variability of precipitation, ground conditions, and vegetation types (Mallick *et al.* 2015). The harsh natural conditions in extreme cold and arid areas make it difficult to obtain sufficient hydrological and meteorological data *in situ*. Despite the urgent need for it, estimating ET_a rates and analyzing the temporal and spatial distribution features of ET_a with limited observation data in extremely cold and arid basins is a tremendous challenge.

Although ET_a can be directly observed by the eddy covariance method, weighing lysimeter method, energy balance Bowen ratio method, or the scintillometer method

doi: 10.2166/nh.2017.104

(Wang & Dickinson 2012; Ma *et al.* 2015b), these all require sufficient manpower, materials, and financial resources. Several approaches to the estimation of ET_a have been developed to date, some of which were derived from the land surface energy balance equation using remotely sensed surface temperatures (e.g., Bastiaanssen *et al.* 1998; Su 2002; Mariotto *et al.* 2011), while others, such as soil-vegetation-atmosphere transfer models, are physically based methods (e.g., Haverd *et al.* 2011) and some are derived from the Penman (1948) or Priestley & Taylor (1972) equations (e.g., Monteith 1965; Allen *et al.* 1998; Monteith & Unsworth 2013). The complementary relationship (CR) between ET_a and potential evaporation (ET_p) was first proposed by Bouchet (1963). Several models based on the CR have been suggested during the past several decades, such as the advection-aridity (AA) model developed by Brutsaert & Stricker (1979), the complementary relationship areal evapotranspiration (CRAE) model of Morton (1983), the Granger model described by Granger & Gray (1989), as well as some nonlinear normalized CR models (Han *et al.* 2012, 2014; Brutsaert 2015; Crago *et al.* 2016; Szilagyi *et al.* 2016, 2017). The CR models are intellectually appealing since they only use routine meteorological data and bypass detailed soil moisture, land cover type, and terrain and vegetation information (Xu & Singh 2005; Ma *et al.* 2015b; Szilagyi *et al.* 2016). The CR approaches have been widely applied over different underlying conditions, spatial scales, and temporal scales (e.g., Xu & Singh 2005; Huntington *et al.* 2011; Wang *et al.* 2011; Han *et al.* 2012, 2014; Crago & Qualls 2013; Mallick *et al.* 2015; Hobbins *et al.* 2016; McEvoy *et al.* 2016). However, one criticism of the CR is the lack of definitive derivation and physical constraints (Crago *et al.* 2016; Szilagyi *et al.* 2016), although some studies have attempted to rectify this (Szilagyi 2007; Han *et al.* 2012, 2014; Brutsaert 2015; Aminzadeh *et al.* 2016; Crago *et al.* 2016; Szilagyi *et al.* 2016, 2017). In addition, there is a strong argument between symmetric and asymmetric CR under different settings (Szilagyi 2007; Jaksa *et al.* 2013; Ma *et al.* 2015b; Crago *et al.* 2016). Han *et al.* (2012) proposed boundary conditions (BCs) in the CR formulation and a new nonlinear function satisfying these BCs. Through comparison of the nonlinear CR developed by Han *et al.* (2012), the CRAE, and the Penman–Monteith approaches, Ma *et al.* (2015b) suggested that the nonlinear CR performed well with limited observation data for local calibration of the model parameter values. Moreover, they found that this CR model had an obvious advantage in both theory and practice in that it did not require users to select a symmetric or asymmetric CR relationship. Brutsaert (2015) reformulated the CR as a general polynomial based on strictly physical considerations. Szilagyi *et al.* (2016) compared the original version of the generalized CR of Brutsaert (2015) with a revised version in which the BCs-(ii) of Brutsaert (2015) was replaced. Furthermore, Crago *et al.* (2016) elaborated why these BCs-(ii) needed to be replaced, and introduced a new concept, the maximum ET_p (denoted by E_{pads} in the literature), to normalize ET_p as $x_{\min}$. They also proposed a new version of the CR based on rescaling, which not only reduced scatter of ET_a estimates, but led to formation of a proposed self-adjusting CR model. Szilagyi *et al.* (2017) redefined the maximum ET_p as an invariable result of adiabatic drying under near-neutral atmospheric conditions (denoted by E_{pmax} in the literature). E_{pads} was calculated by the mass-transfer-based method, while E_{pmax} was calculated by the Penman-based equation (Ma & Zhang 2017). How to define the maximum ET_p could be the key to the application of the modified Brutsaert (2015) generalized CR model by Crago *et al.* (2016) and Szilagyi *et al.* (2017).

In recent years, the rapid development of satellite remote sensing has led to remote sensing data providing great convenience for spatio-temporal samplings (Singh *et al.* 2008; Liu *et al.* 2009). However, reanalysis-based methods (Mesinger *et al.* 2006; Yang *et al.* 2010; Lavers *et al.* 2012) have unique advantages, such as less sensitivity to cloud cover, longer temporal coverage, and better representation of actual conditions for spatially distributed data (Szilagyi *et al.* 2017). The China Meteorological Forcing Dataset is a reanalysis dataset of surface meteorological and environmental factors developed by the Institute of Tibetan Plateau Research, Chinese Academy of Sciences. Using Princeton reanalysis forcing data, Global Land Data Assimilation System data, Global Energy and Water Exchanges-Surface Radiation Budget data, and Tropical Rainfall Measuring Mission data (3B42) as the background, this dataset also combines China Meteorological Administration station data from 1979 to 2015. The spatial resolution of this dataset is 0.1° and its temporal resolution is 3 h (He & Yang 2011).

The Hotan River Basin (HRB) is located in the hinterland of the Taklimakan Desert of northwest China (the largest desert in China) and at the north side of the Kunlun Mountains (part of the Tibetan Plateau). There are limited observation data available for extreme cold and arid areas of the river basin. In this study, the modified generalized CR framework of Crago *et al.* (2016), with the maximum ET_p defined by Crago *et al.* (2016) and Szilagyi *et al.* (2017), was applied to estimate the daily ET_a rates in the HRB from 2006 to 2013. The China Meteorological Forcing Dataset was used to calculate the CR components and analyze regional water balance, while Moderate Resolution Imaging Spectroradiometer (MODIS) data were used to calculate the net solar radiation (R_n). The daily precipitation data and monthly runoff data were collected to calculate a regional water budget. The objectives of this study were: (i) to analyze the improvement effects of different modified methods and select an appropriate definition of the maximum ET_p according to conditions in the study basin; (ii) to calibrate the local parameter values of the Priestley–Taylor coefficient α and the adjustable parameter σ to estimate daily ET_a rates and validate the annual ET_a by using a regional water balance; and (iii) to evaluate the temporal and spatial distribution variations of ET_a and the water budget in the HRB during 2006–2014.

MODEL AND PARAMETERIZATION

Background of the CR

The CR theory proposed by Bouchet (1963) can be described as follows (Brutsaert & Parlange 1998):

$$ET_p - ET_w = b(ET_w - ET_a), \tag{1}$$

where ET_w is the wet-environment evaporation, and b is a proportionality parameter. The CR postulates that opposite changes exist between ET_a and ET_p, meaning that when soil moisture decreases and the available energy remains constant, the energy would have been consumed by ET_a, while when soil moisture is saturated, $ET_a = ET_p = ET_w$. Note that the symmetric CR postulated by Bouchet (1963) implies b equals unity (Aminzadeh & Or 2017). The AA model or modified AA models with $b = 1$ have achieved good performance (Xu & Singh 2005; Hobbins *et al.* 2001; Ma *et al.* 2015b; Szilagyi 2015). Nevertheless, under many conditions reported in the literature, b is considerably larger than 1 (Aminzadeh & Or 2017), and is even thought to be variable (Granger & Gray 1989; Szilagyi 2007; Han *et al.* 2012).

In the most widely used AA model, ET_p should be estimated using the Penman (1948) equation and ET_w should be estimated using the Priestley–Taylor (1972) equations:

$$ET_p = \frac{\Delta}{\Delta+\gamma}\frac{(R_n - G)}{\lambda} + \frac{\gamma}{\Delta+\gamma}f(U)(e_s - e_a), \tag{2}$$

$$ET_w = \alpha\frac{\Delta}{\Delta+\gamma}\frac{(R_n - G)}{\lambda}, \tag{3}$$

where Δ is the slope of the saturation vapor pressure curve at the air temperature (kPa $^\circ C^{-1}$); γ is the psychometric constant (kPa $^\circ C^{-1}$); R_n is the net radiation (MJ m^{-2} day^{-1}); G is the soil heat flux (MJ m^{-2} day^{-1}); λ is the latent heat of vaporization (MJ kg^{-1}); e_s is the saturation vapor pressure at air temperature (kPa); e_a is the actual vapor pressure (kPa); (e_s–e_a) is the saturation vapor pressure deficit (kPa); and α is the coefficient with a default value of approximately 1.26, which depends mainly on underlying surface conditions (Brutsaert 2015). In the present study, the values of α were recalculated based on underlying surface conditions. Additionally, *f (U)* is a function of the mean wind speed at a reference level (mm day^{-1} kPa^{-1}), which is either theoretically or empirically derived. The Penman's (1948) empirical linear *f (U)* is commonly used (Brutsaert 1982; Qualls & Gultekin 1997; Xu & Singh 2005):

$$f_P(U) = 2.6(1 + 0.54U_2), \tag{4}$$

where U_2 is the wind speed (m s^{-1}) at a height of 2 m.

As demonstrated by Hobbins *et al.* (2001) and Ma *et al.* (2015b), Equation (4) should be replaced with a more appropriate method to accurately estimate ET_p. At daily or longer time scales, atmospheric stability is generally considered to be neutral (Ma *et al.* 2015b). Brutsaert & Stricker (1979) suggested that the *f (U)* should be derived through the

Monin–Obukhov similarity theory as follows:

$$f_M(U) = \frac{0.622k^2\rho U_2}{P_a \ln(z - d/z_{ov}) \ln(z - d/z_{om})} t, \quad (5)$$

where $t = 86{,}400\ s$; $k = 0.4$ is the von Karman constant; ρ is the density of air (kg m^{-3}); P_a is the air pressure (kPa); z is the measurement height of wind speed and humidity (2 m in this study); d is the displacement height (m); and z_{om} and z_{ov} are the roughness lengths of momentum and water vapor (m), respectively. z_{om} and d are correlated with the effective vegetation height, h (Guo & Shen 2015). For trees, $z_{om} = 0.075\ h$ and $d = 0.78\ h$ (Guo & Shen 2015); for cropland and grass, $z_{om} = 0.123\ h$ and $d = 0.67\ h$ (Allen *et al.* 1998); for urban and barren land, $z_{om} = 0.004$ m (Wang *et al.* 1988; Han *et al.* 2012). Finally, z_{ov} can typically be expressed as $z_{ov} = 0.14\ z_{om}$ (Ryu *et al.* 2008; Ma *et al.* 2015b).

Szilagyi & Jozsa (2008) suggested that Δ in Equation (3) should be evaluated at the wet environment air temperature (T_w) rather than air temperature (T_a). This modification is necessary to estimate T_w in arid or semiarid regions because of the large difference between T_w and T_a (Huntington *et al.* 2011; Szilagyi 2014). T_w is generally unknown for water-limited conditions, but can be approximated by the wet environment surface temperature (T_{ws}) (Huntington *et al.* 2011). Szilagyi & Jozsa (2008) recommended an implicit equation for T_{ws} based on the Bowen ratio (B_o) for a small wet patch:

$$B_o = \frac{((R_n - G)/(\lambda - ET_p))}{ET_p} \approx \gamma \frac{T_{ws} - T_a}{e_o(T_{ws}) - e_a}, \quad (6)$$

where $e_o(T_{ws})$ is the saturated vapor pressure at T_{ws} (K). T_{ws} can be solved through iterations. Normally, for a small wet surface, T_{ws} is typically lower than T_a; thus, T_{ws} calculated by Equation (6) can be taken for T_w. If $T_{ws} > T_a$, T_w should be replaced by T_a (Huntington *et al.* 2011; Szilagyi 2014; Ma *et al.* 2015b).

Actual vapor pressure (e_a) has a good correlation with dew point temperature, relative humidity, specific humidity, dry bulb temperature, or wet bulb temperature. e_a can be approximated as follows:

$$e_a = \frac{qP_a}{0.622}, \quad (7)$$

where q is the specific humidity (kg kg^{-1}).

Utilizing the Surface Energy Balance System method of Su (2002), R_n was calculated using remote sensing data as an instantaneous value. The daily R_n values were estimated by implementing the sinusoidal model given by Bisht *et al.* (2005). The other climate-related parameters, G, e_s, λ, Δ, ρ_a, c_p, and γ, were calculated using the method recommended by the Food and Agriculture Organization (Allen *et al.* 1998).

Generalized CR and theoretical development

The dimensionless form of the AA model with ET_p is formed from combining Equation (1) with Equations (2) and (3):

$$\frac{ET_a}{ET_p} = \left(1 + \frac{1}{b}\right)\frac{ET_w}{ET_p} - \frac{1}{b}. \quad (8)$$

Equation (8) generates the dimensionless variables $y = ET_a/ET_p$ and $x = ET_w/ET_p$. Values of y and x are between 0 and 1. Equation (8) becomes

$$y = \left(1 + \frac{1}{b}\right)x - \frac{1}{b}. \quad (9)$$

Brutsaert (2015) imposed four BCs by setting physical constraints to develop a fourth-order polynomial relationship between y and x that was inspired by Han *et al.* (2012). The four BCs are as follows: (i) $y = 1$ at $x = 1$; (ii) $y = 0$ at $x = 0$; (iii) $dy/dx = 1$ at $x = 1$; and (iv) $dy/dx = 0$ at $x = 0$. However, Szilagyi *et al.* (2016) recommended that BCs-ii should be replaced by $y = 0$ at $x = x_{\min}$. To calculate $x_{\min}$, Crago *et al.* (2016) introduced the maximum ET_p (hereinafter ET_{pmax}) and recommended that ET_{pmax} be obtained from a small wet surface according to the aerodynamic mass transfer equation, denoted by ET_{pds} in the present study:

$$ET_{pds} = \frac{[q*(\mathrm{T_{ws}}) - 0]\mathrm{k}^2\rho\mathrm{U}_2}{\ln((z - d)/(z_{ov}))\ln((z - d)/(z_{om}))} t, \quad (10)$$

where $q*(\mathrm{T_{ws}})$ refers to saturated specific humidity at T_{ws}. The specific humidity, $q = 0$ at height z. In the present study, $z = 2$ m. Substituting Equation (5) into Equation (10), one obtains the following:

$$ET_{pds} = f_M(U)e^o(T_{ws}), \quad (11)$$

where $e^o(T_{ws})$ is the saturation vapor pressure at T_{ws}.

As an alternative, $ET_{p\max}$ could also be obtained from the Penman equation with $e_a = 0$, and the temperature for a dry surface (denoted by T_{dry}), denoted by ET_{pdry} in the present study, can be obtained according to the definition by Szilagyi *et al.* (2017):

$$ET_{pdry} = \frac{\Delta(T_{dry})}{\Delta(T_{dry}) + \gamma}\frac{R_n}{\lambda} + \frac{\gamma}{\Delta(T_{dry}) + \gamma} f_M(U) e^o(T_{dry}), \quad (12)$$

where $\Delta(T_{dry})$ is the slope of the saturation vapor pressure curve at T_{dry}, and T_{dry} is defined for adiabatic changes as $T(e_a = 0) = T_{dry}$. T_{dry} is described in more detail by Szilagyi (2014) and Szilagyi *et al.* (2017).

Once $ET_{p\max}$ has been determined by employing Equation (11) or Equation (12), $x_{\min}$ can be obtained using the formula given by Crago *et al.* (2016):

$$x_{\min} = \frac{ET_w}{ET_{p\max}}. \quad (13)$$

Crago *et al.* (2016) suggested that $x = x_{\min}$ is the lower boundary of the CR, so the CR could be formulated by rescaling x:

$$X = \frac{x - x_{\min}}{1 - x_{\min}}. \quad (14)$$

Considering the special geographical situation, such as the significant elevation change or the different underlying conditions, some flexibility in CR formulations may be needed (Crago *et al.* 2016). As recommended by Crago *et al.* (2016), a general polynomial function can be sought in the form of

$$y = a_0 + a_1 X + a_2 X^2 + a_3 X^3. \quad (15)$$

We might specify four BCs inspired by Brutsaert's (2015): (i) y = 1 at X = 1; (ii) y = 0 at X = 0; (iii) dy/dX = 1 at X = 1; (iv) dy/dX = σ at X = 0. Equation (15) becomes

$$y = \sigma X + (2 - 2\sigma)X^2 + (\sigma - 1)X^3 \quad (16)$$

containing only one adjustable parameter σ. When $\sigma = 1$, Equation (16) reduces to $y = X$ as used by Crago *et al.* (2016). When $\sigma = 0$, Equation (16) reduces to $y = 2X^2 - X^3$ as used by Szilagyi *et al.* (2017).

STUDY AREA AND DATA

Study area

The HRB is located in northwest China (77.40°E–81.59°E, 34.84°N–40.44°N), covering an area of 88,753 km^2 (draining to the Xiaota hydrological station) (Figure 1). The HRB is one of the main headwaters of the Tarim River, which is the largest inland river in China. The altitude of the HRB varies between 1,014 m and 6,858 m above sea level (asl) (Figure 1). The source of the Hotan River is located at the north side of the Kunlun Mountains, and the lower reaches pass through the hinterland of the Taklimakan Desert. The mountainous regions (above 2,000 m asl) are covered with ice and snow, alpine grasslands, and bare rock (Figure 2), and are characterized by a frigid arid climate (Zheng *et al.* 2013). The plains regions (below 2,000 m asl) are mainly covered with croplands, desert steppes, and desert (Figure 2). The oasis-desert systems are characterized by a warm temperate arid climate (Zheng *et al.* 2013). Because of the colossal irrigation system in the HRB, drainage collects downstream of the irrigated area, where an oasis-desert transition area is formed. The Kalakashi River and the Yulongkashi River are two branches of the Hotan River that cross the Hotan oasis. There are only two meteorological stations in the Hotan oases and five hydrological stations on the Hotan River (Figure 1). All of these stations are at less than 2,000 m asl, and there are no stations in the mountainous regions or desert regions of the HRB. Two mountain-pass hydrological stations, Wuluwati and Tonguziluoke, are at around 2,000 m asl. The Aigeliya and Tuzhiluke hydrological stations are at the convergence of the two branches. The Xiaota hydrological station is at 319 km downstream of the convergence, which is the single basin export to the Tarim River (Zhao *et al.* 2009; Lyu *et al.* 2015).

Data description

In the present study, 0.1° grid-based meteorological data of the China Meteorological Forcing Dataset in the HRB

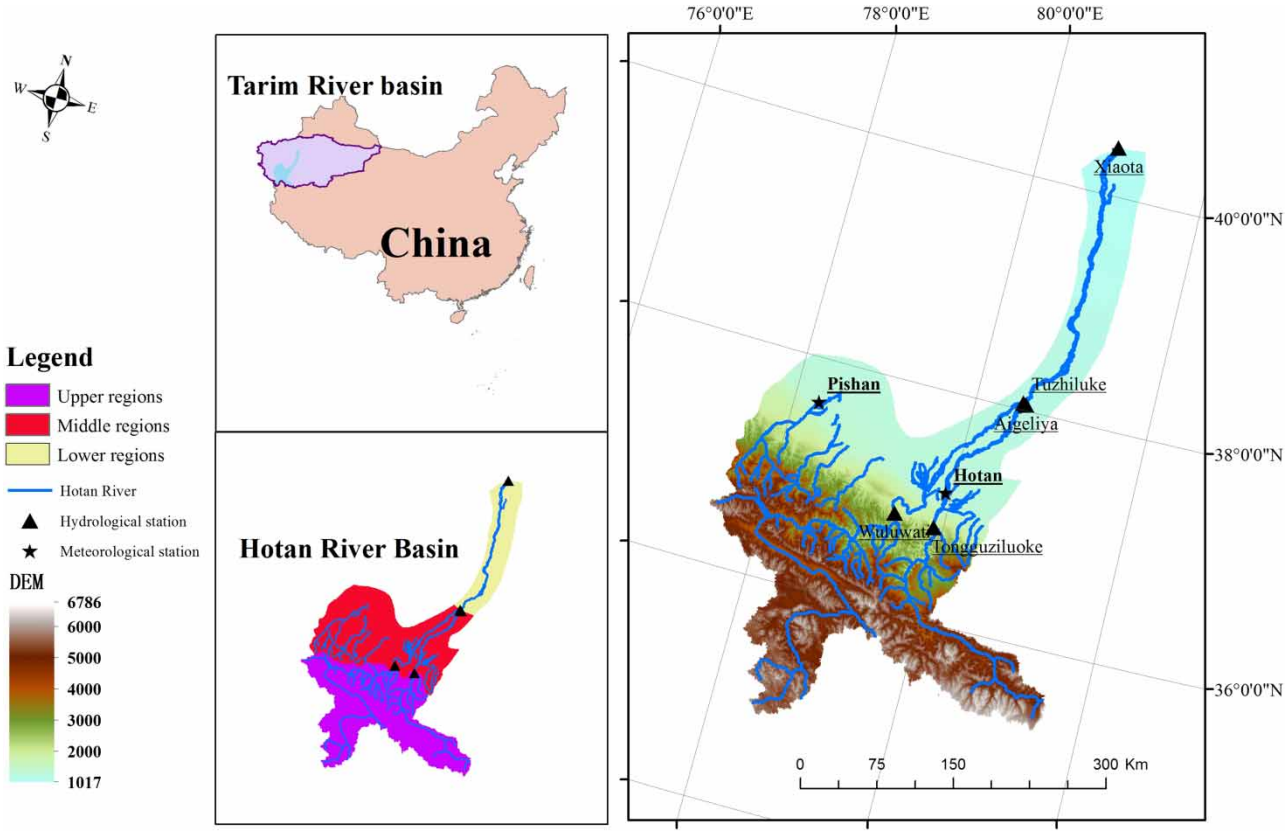

Figure 1 | Location of the study basin and the hydrological and meteorological stations. The HRB is divided into three parts (the upper, middle, and lower regions) according to the location of hydrological stations.

during 2006–2014 were used, including mean daily air temperature, mean specific humidity, mean wind speed, precipitation, and 3-hourly mean air temperature. As mentioned in the Introduction, the China Meteorological Forcing Dataset was produced by merging a variety of data sources (He & Yang 2011). This study used 3-hourly mean temperature from this dataset to facilitate the preparation of daily maximum and minimum temperatures. Note that the wind speed in this dataset was at a height of 10 m (U_{10}); therefore, U_{10} values were transformed to U_2 values via $U_2 = 0.748\,U_{10}$ (Allen *et al.* 1998). We also used MODIS data at a spatial resolution of 1 km, including MOD11A2 (emissivity, land surface temperature), MCD43B3 (albedo), MCD15A2 (leaf area index), and MCD12Q1 (land cover type). Additionally, digital elevation model (DEM) data of approximately 90 m resolution were collected. The forcing datasets and DEM data were used with the cubic convolution resampling technique to attain the 1 km spatial resolution matching the remotely sensed data. MODIS data collected at 8-day time steps was linearly interpolated to obtain daily values. Spatio-temporal gap filling of missing data during cloudy periods was accomplished through compositing time series data (Cleugh *et al.* 2007). Moreover, the monthly runoff data from the five hydrological stations were collected to analyze regional water balance.

RESULTS AND ANALYSES

Testing different versions of key parameters

In the above description, $f_P(U)$ was replaced by $f_M(U)$, and Δ in Equation (3) was evaluated at T_w rather than at T_a. In this section, the improvement effects of different modified methods were analyzed. In addition, the two definitions of ET_{pmax} of Crago *et al.* (2016) and Szilagyi *et al.* (2017)

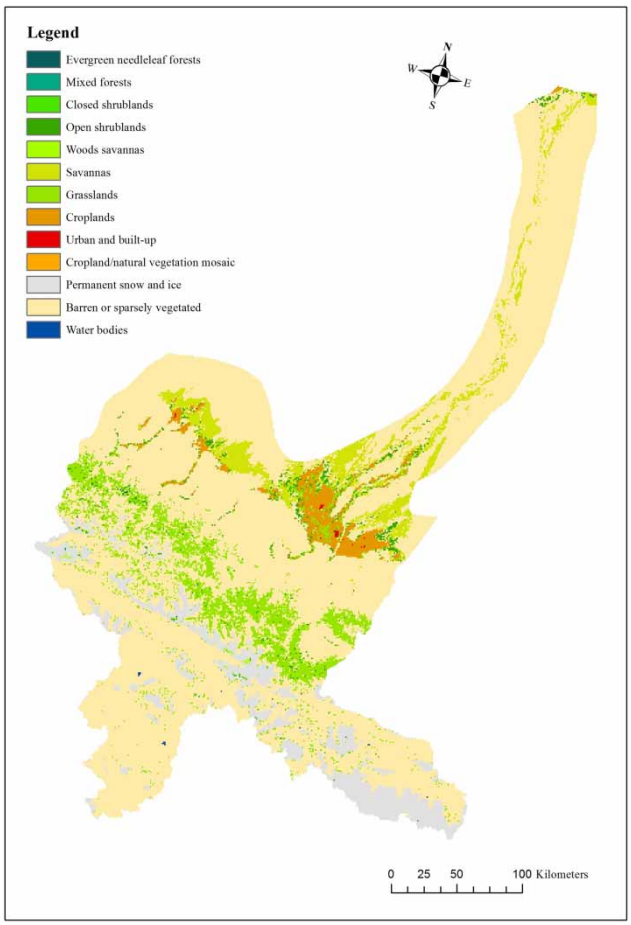

Figure 2 | Land use/cover in the HRB in 2011.

described above, were compared and selected according to conditions in the study basin. Analysis of annual precipitation data from 2006 to 2014 revealed that the precipitation in 2011 was in the median value. Therefore, 2011 was chosen as an example to represent the climate of the study region.

As shown in Figure 3(a) and 3(b), the spatial distribution of the daily mean wind function derived from Equation (4) ($f_P(U)$) was compared with that derived from Equation (5) ($f_M(U)$). The mean value of $f_M(U)$ (3.11 mm day^{-1} kPa^{-1}) was smaller than the mean value of $f_P(U)$ (4.54 mm day^{-1} kPa^{-1}). The spatial distribution of the absolute percentage difference (APD) between $f_M(U)$ and $f_P(U)$ (denoted by APD_f (U)), as well as the spatial distribution of the APD between ET_p derived from $f_M(U)$ and that derived from $f_P(U)$ (denoted by APD_ET_p) can be seen in Figure 3(c) and 3(d). The mean values of APD_f (U) and APD_ET_p were 0.32 and 0.23, respectively, with larger values in the plains regions than in the mountainous regions. Moreover, the values of APD_ET_p in desert regions were larger than those in oasis regions. These results indicate that the correction of the wind function had a more significant reduced-ET_p effect in the plains regions than in the mountainous regions, while the correction of the wind function to the estimate of ET_p had the most significant influence in desert regions of the plains regions, followed by influence in oasis regions of the plains regions; meanwhile, it had the least influence in the mountainous regions.

Figure 4(a) and 4(b) display the spatial distribution of the daily mean T_a and the daily mean T_w, respectively. The spatial distribution of the mean absolute error (MAE) between T_a and T_w (denoted by MAE ($T_a - T_w$)), and the MAE between ET_{rad} derived at T_a and that derived at T_w (denoted by MAE (ET_{rad})) can be seen in Figure 4(c) and 4(d). The values of MAE ($T_a - T_w$) in the plains regions were larger than those in the mountainous regions, while those in oasis-desert transition regions were larger than those values in desert and/or oasis regions. The spatial distribution of MAE (ET_{rad}) was similar to the distribution of MAE ($T_a - T_w$). The correction of T_w to the estimate of ET_{rad} had a relatively small influence, with the maximum MAE (ET_{rad}) value of 32.87 mm (about 3.5% of the ET_{rad} derived at T_a).

Figure 5(a) and 5(b) show the spatial distribution of the annual ET_{pds} estimated from Equation (11) and the annual ET_{pdry} estimated from Equation (12), respectively. Figure 5(c) and 5(d) display the spatial distribution of the difference between ET_{pds} and ET_p (denoted by $ET_{pds} - ET_p$) and the difference between ET_{pdry} and ET_p (denoted by $ET_{pdry} - ET_p$), respectively. The values of $ET_{pds} - ET_p$ in the plains regions were greater than 0, while those in the mountainous regions were less than 0. These results indicated that ET_{pds} was less than ET_p in the mountainous regions. According to the basic assumptions of Crago *et al.* (2016), $ET_w \le ET_p \le ET_{p\max}$, and the $ET_{p\max}$ defined by Crago *et al.* (2016), i.e., ET_{pds}, was not applicable in the study basin, especially in the mountainous regions. However, the values of $ET_{pdry} - ET_p$ were greater than 0 in the whole basin, with the minimum value of 170.2 mm yr^{-1} in the mountainous regions and the maximum value of 660.2 mm yr^{-1} near Xiaota station in the plains regions. Therefore, $ET_{p\max}$ defined by Szilagyi *et al.* (2017), i.e., ET_{pdry}, should be adopted in the present study.

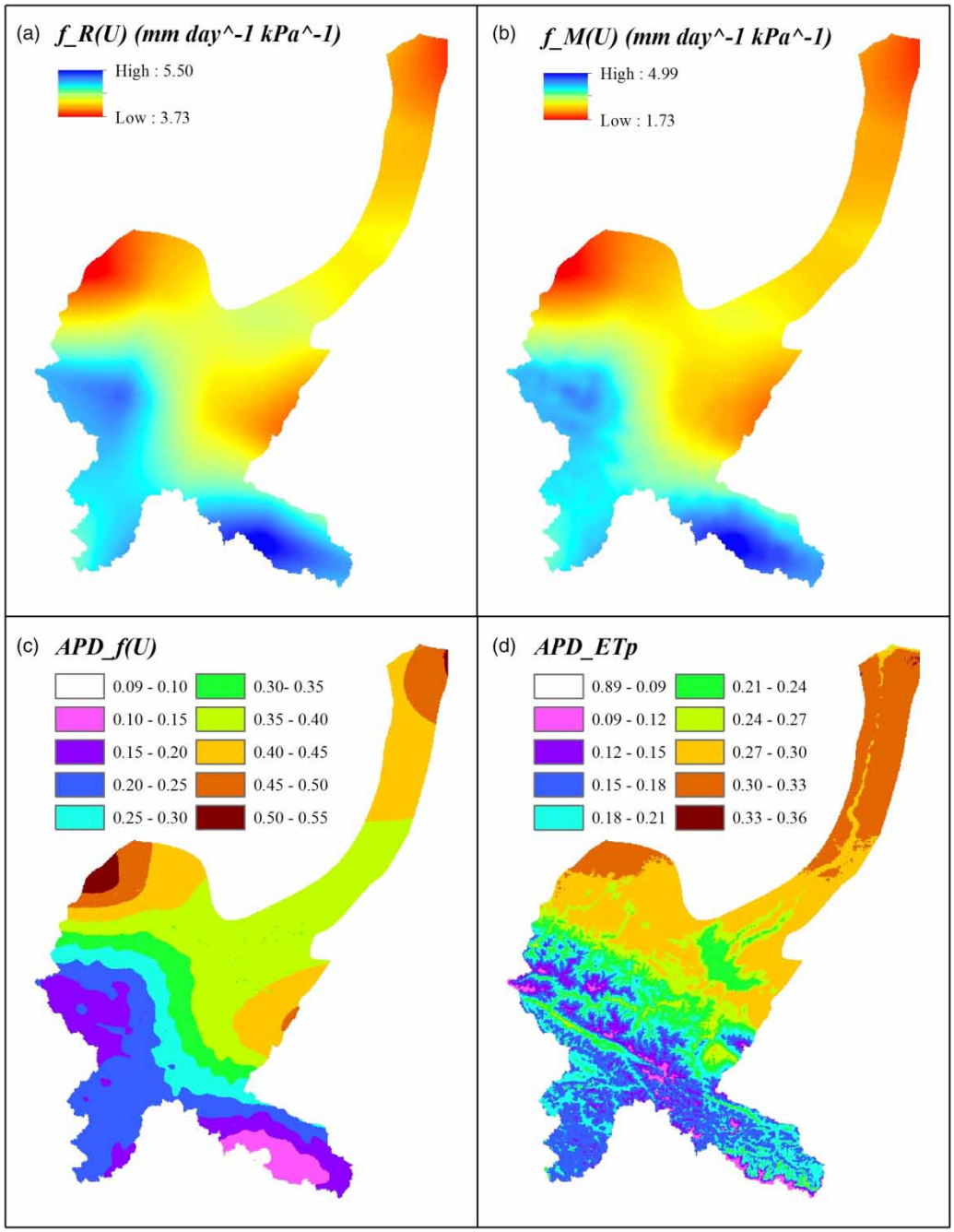

Figure 3 | Spatial distribution of (a) the daily mean wind function derived from Equation (4) ($f_P(U)$) and (b) the daily mean wind function derived from Equation (5) ($f_M(U)$); (c) the *APD* between $f_P(U)$ and $f_M(U)$ (denoted by *APD_f* (U)) and (d) the *APD* between ET_p derived from Equation (4) and that derived from Equation (5) (denoted by APD_ET_p) in 2011 as an example.

Calibration and validation

Priestley & Taylor (1972) and subsequent studies have suggested a value of the Priestley–Taylor coefficient α in Equation (3) near 1.26 with a narrow range (e.g., Eichinger *et al.* 1996; Crago *et al.* 2010). Hobbins *et al.* (2001) obtained a value of $\alpha = 1.3177$ using data from 92 basins of the USA. Brutsaert (2005) suggested that α for saturated

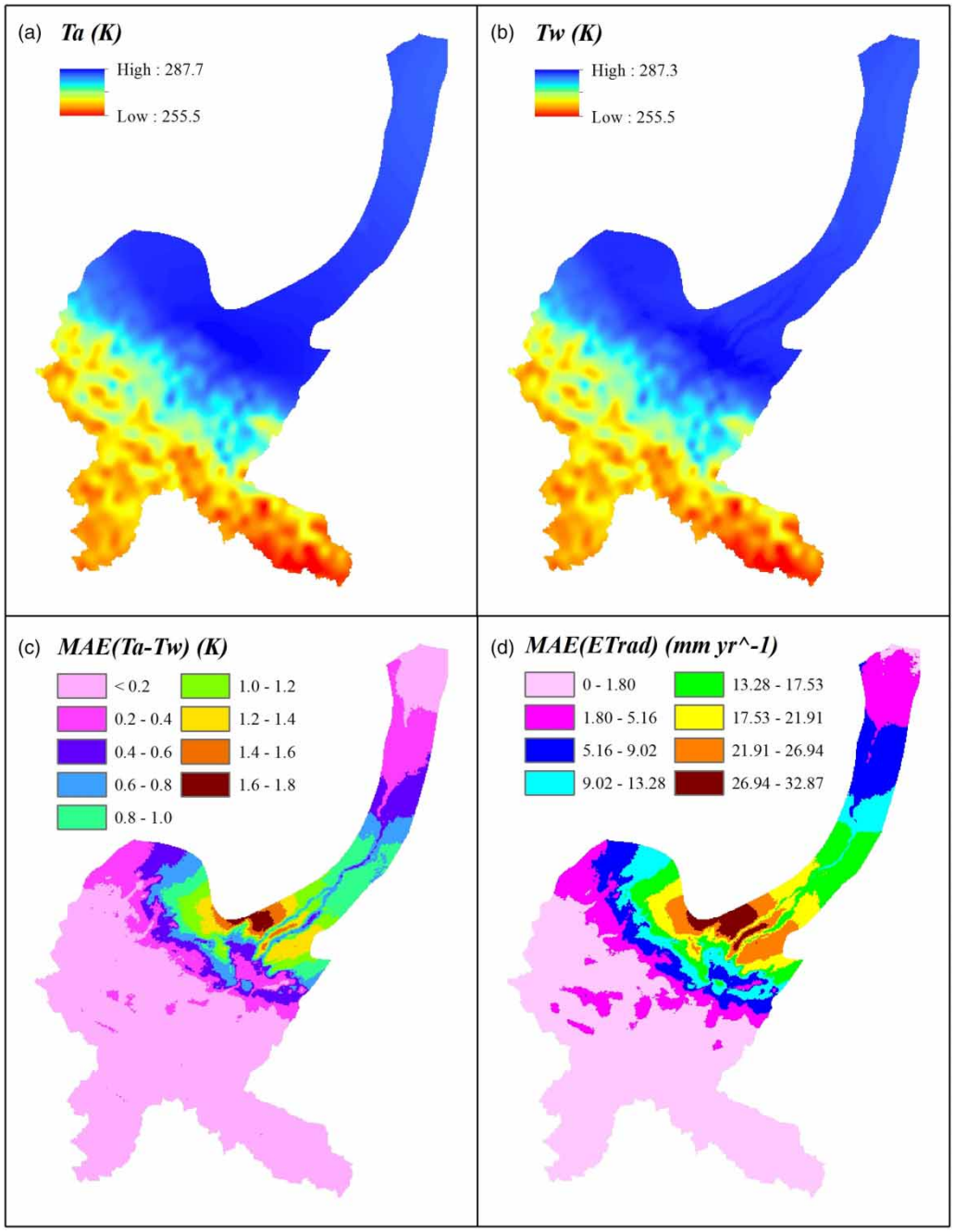

Figure 4 | Spatial distribution of (a) the daily mean air temperature (T_a) and (b) the daily mean wet environment air temperature (T_w); (c) the *MAE* between T_a and T_w (denoted by *MAE* ($T_a - T_w$)) and (d) the *MAE* between ET_{rad} derived at T_a and that derived at T_w (denoted by *MAE* (ET_{rad})). The year 2011 is used as an example.

surfaces typically falls between 1.20 and 1.30. Xu & Singh (2005) determined α values for three study regions at 1.18, 1.04, and 1.00. Yang *et al.* (2008) obtained an average $\alpha =$ 1.17 with a range of 0.87–1.48 from 108 basins of China, whereas Gao *et al.* (2012) suggested α falls between 1 and 1.23 for nine sub-basins of the Haihe River Basin. Similar seasonal variability for α in the range of 1.1–1.4 was reported for the Asian monsoon (Yang *et al.* 2013). Brutsaert (2015) and Ma *et al.* (2015b) used α near 1.13. The α value was also reported to be a function of the water content

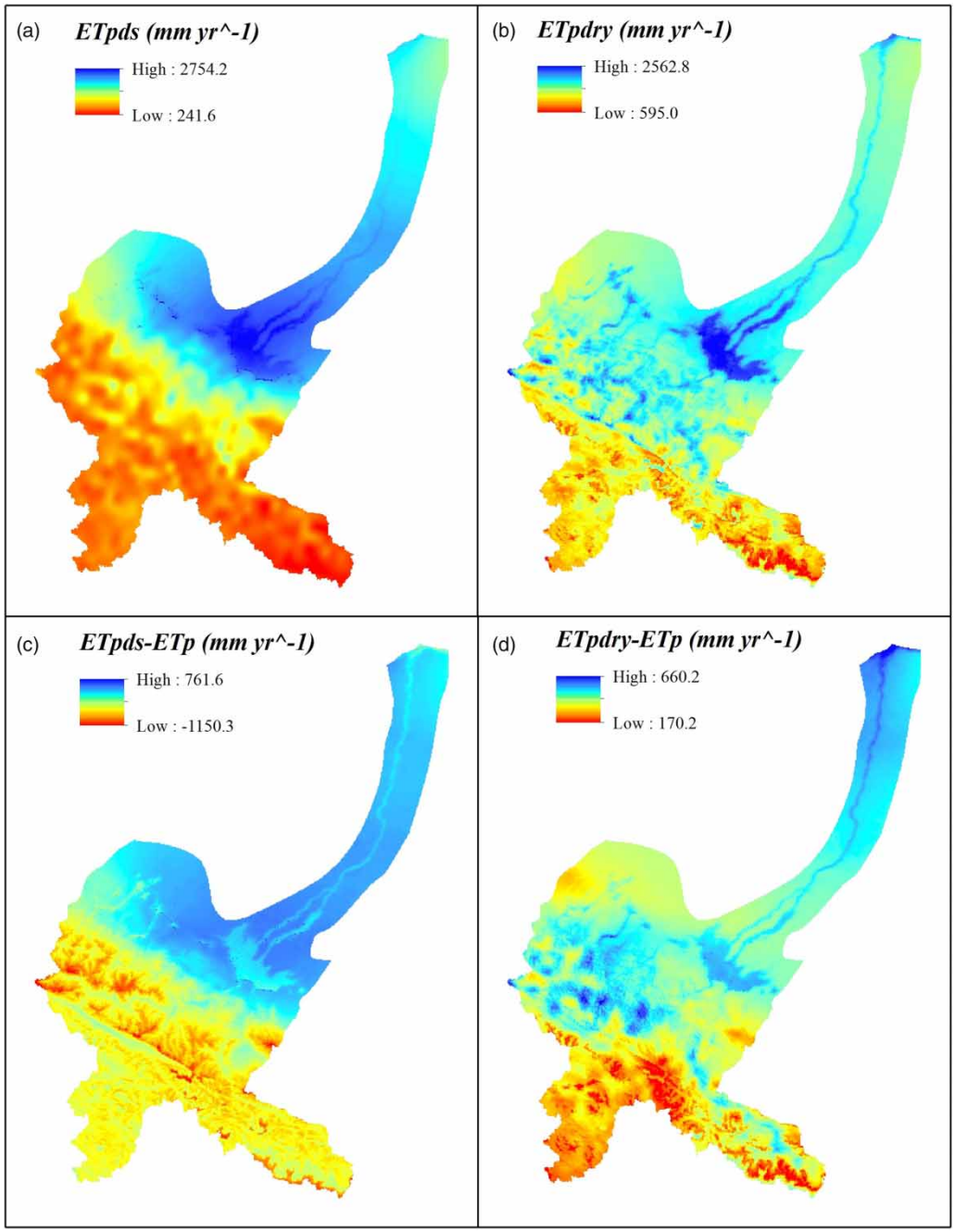

Figure 5 | Spatial distribution of (a) annual ET_{pds} estimated from Equation (11) and (b) annual ET_{pdry} estimated from Equation (12); (c) the difference between ET_{pds} and ET_p (denoted by $ET_{pds} - ET_p$) and (d) the difference between ET_{pdry} and ET_p (denoted by $ET_{pdry} - ET_p$). The year 2011 is used as an example.

of drying soil surfaces, reaching values as low as 0.25 for relatively dry soil surfaces (Aminzadeh & Or 2014). To accommodate the observed range of α, we assume $1 \leq \alpha \leq 1.32$. Szilagyi *et al.* (2017) proposed a novel approach to obtain the value of α that applied to a calibration-free formulation of the CR. However, their approach to obtain the value of α is unsuitable in extreme cold and arid basins. Due to the lack of measured data, a value of α cannot be accurately determined. However, the fact that $ET_w \leq ET_p$ can estimate the possible maximum

value of α, thus, $1 \leq \alpha \leq 1.07$ for the HRB. We assume that a fixed value of α is applicable in the whole basin, even though we agree with the view that α changes over time and underlying surface. Hence, we assume that $\alpha = 1.07$ for the HRB in the present study. In addition, we assume that $ET_a = 0$ when T_a is less than the dew point temperature.

The adjustable parameter σ in Equation (16) was treated as the only calibration parameter. Note that one can deduce from Equation (16) that ET_a rates increase monotonously as the σ value increases. Because measured data for the HRB in extreme cold and arid areas were limited, the calculated results were not verified at daily and monthly time scales. Therefore, the calibration of σ and the validation of ET_a used the regional water balance method at annual time scales.

ET_a estimated from the water balance equation (ET_{wb}) was used as the reference at annual time scales:

$$ET_{wb} = P - R + \Delta W, \tag{17}$$

where P is the annual precipitation; R is the annual runoff; and ΔW denotes the water storage change, which includes groundwater, glacial water, and soil moisture. ΔW was assumed to be 0 at the annual time scale in the present study because the accurate water storage change data were almost impossible to obtain in the HRB, there was not much groundwater extracted for irrigation, and the change of water storage was small in the calibration period (just one year in the present study). Considering the severe spatio-temporal heterogeneity between precipitation and ET_a, the HRB was divided into upper, middle, and lower regions to calibrate the coefficient σ and verify ET_a rates according to the location of hydrological stations (Figure 1). The year 2011 was chosen to determine the optimal values of α because it was neither too wet nor too dry, while other years were used as the validation period.

Calibration was conducted as follows. First, the coefficient σ in desert or urban regions of the plains regions was determined since precipitation does not produce runoff and is almost completely evaporated (Ma *et al.* 2014). Second, the coefficient σ in vegetated areas of the plains regions was determined according to the regional water balance method. Third, the coefficient σ in rock bare regions of the mountainous regions was determined. Considering that the daily maximum temperature was less than 0 °C above 5,000 m asl during most of the year, ET_a rates above 5,000 m asl were quite low. As mentioned above, ET_a rates increased monotonously with increasing σ; therefore, we assumed that the values of σ decreased monotonously with increasing elevation. For conveniently calibrating, elevation of the mountainous regions was divided into three parts, and we assumed that the relationship between σ and elevation was linear in each elevation interval. Note that the relationship between σ and elevation might be actually nonlinear. Finally, the coefficient σ in vegetated areas of the mountainous regions was determined using a method similar to that employed for the rock bare regions. The optimal values of σ used for Equation (16) were found (Table 1) by minimizing the sum of absolute errors ($MSAE$) between ET_{wb} and ET_a. The optimal values of σ were applied to estimate ET_a in the validation period, and the results are listed in Table 2. Note that Zhao *et al.* (2009) obtained mean annual evapotranspiration (198.78 mm) from year 1954 to 2003 in middle regions. In this study, the mean annual evapotranspiration in middle regions was 209.2 mm which is very close to the results of Zhao *et al.* (2009).

Table 1 | Values of optimized parameter σ in the upper, middle, and lower regions

	Vegetated regions			Unvegetated regions		
Elevation (m asl)	**ET_p (mm)**	**P (mm)**	**σ**	**ET_p (mm)**	**P (mm)**	**σ**
<1,200	1,287.17	81.56	−3.2	1,239.99	83.09	−7
1,200–2,000	1,560.45	51.89	0.6	1,343.87	82.04	−4.2
2,000–3,000	1,278.33	161.3	100 − 50*(Elevation/1,000)	1,258.84	148.99	82 − 44*(Elevation/1,000)
3,000–4,000	1,256.35	182.85	400 − 150*(Elevation/1,000)	1,168.83	188.92	700 − 250*(Elevation/1,000)
>4,000	1,156.5	196.94	400 − 150*(Elevation/1,000)	1,006.5	196.15	1,300 − 400*(Elevation/1,000)

Table 2 | Annual precipitation (*P*), runoff (*R*), ET_{wb}, ET_a, and *MSAE* in the upper, middle, and lower regions during 2006–2014

	Upper regions				Middle regions				Lower regions				
Year	*P*	*R*	ET_{wb}	ET_a	*P*	*R*	ET_{wb}	ET_a	*P*	*R*	ET_{wb}	ET_a	*MSAE*
2011	183.74	137.44	46.30	46.39	104.95	−104.43	209.38	209.95	82.93	−61.14	144.07	144.80	1.39
2006	225.59	163.72	61.87	48.79	155.87	−94.42	250.30	233.43	78.54	−58.48	137.01	119.13	−47.83
2007	156.60	117.01	39.59	34.44	79.89	−98.46	178.36	155.87	59.58	−44.53	104.11	93.30	−38.45
2008	186.33	121.89	64.44	46.42	83.66	−109.21	192.87	166.52	70.15	−33.60	103.75	121.07	−27.05
2009	123.17	98.29	24.88	38.71	54.80	−87.39	142.19	141.58	67.85	−33.16	101.02	91.45	3.65
2010	237.17	182.98	54.19	53.55	202.07	−104.12	306.18	257.54	149.00	−96.30	245.30	156.11	−138.47
2012	204.86	162.99	41.87	62.12	105.38	−108.69	214.07	298.03	88.04	−55.03	143.07	182.51	143.65
2013	247.13	201.91	45.22	46.06	113.08	−126.02	239.10	220.79	114.85	−46.82	161.67	151.49	−27.65
2014	194.09	134.69	59.40	48.20	82.86	−99.11	181.96	199.86	70.53	−41.16	111.69	135.04	30.05
Mean	196.87	147.94	48.93	47.25	109.70	−103.43	213.13	209.20	87.32	−51.14	138.45	131.26	−12.8

Note that *R* refers to a ratio of the difference in runoff volume observed between the downstream and upstream hydrological stations to region area; and Mean refers to the mean annual value during the validation period (all in mm yr^{-1}).

In general, the mean annual ET_a estimated using the optimal values of α matched well with the mean annual ET_{wb}, which indicates that the *MSAE* in the validation period was −12.8 mm yr^{-1}. However, this does not necessarily indicate that the annual *MSAE* was also small. Indeed, there was a certain deviation between the annual ET_a and annual ET_{wb} with the maximum *MSAE* value of 143.65 mm in 2010.

Spatial and temporal variations in precipitation, ET_a, and water budget

Figure 6 shows the spatial distribution of annual ET_a, and Figure 7 shows the spatial distribution of mean annual precipitation, ET_a, and $P - ET_a$ difference during 2006–2014 in the HRB. The mean annual precipitation ranged from 46.0 mm to 342.0 mm, while the mean annual ET_a ranged from 2.3 mm to 800 mm. The higher precipitation values were in the mountainous regions, indicating that the mean annual precipitation was higher at high elevation. ET_a rates in the plains regions were higher than those in the mountainous regions, with the highest values being observed in croplands and shrublands along the riverside. Perhaps the irrigation or groundwater plays a key role in this issue. Relatively lower ET_a occurred in ice and snow regions, as well as in barren land of the mountainous regions. The difference ($P - ET_a$) reflects water surplus or deficits (Figure 7(c)). The mean annual $P - ET_a$ difference in the mountainous regions was positive (except in alpine grasslands), while it was negative in the plains regions. These findings indicate that a great deal of precipitation and runoff dissipated in the form of ET_a in the plains regions.

Figure 8 shows the monthly mean P, ET_a, and $P - ET_a$ difference from 2006 to 2014 in the upper, middle, and lower regions. As shown in Figure 8(a), most of the P was concentrated in the months of May to September, accounting for 65% (128 mm) of annual P in the upper regions, 61% (66 mm) in the middle regions, and 70% (61 mm) in the lower regions. As shown in Figure 8(b), the variations in ET_a in different regions were similar, following a single peak normal distribution. Most of ET_a was concentrated in the months of May to September, accounting for 89% of the mean annual ET_a (42 mm) in the upper regions, 76% (159 mm) in the middle regions, and 80% (105 mm) in the lower regions. The inter-annual changes in ET_a in winter months were lower than in summer months. As shown in Figure 8(c), a water deficit occurred in the middle and lower regions, and a water surplus occurred in the upper regions. Because the inter-annual changes in P were relatively large, the inter-annual changes in water budget were relatively large as well. Water deficits occurred during most months throughout the year in the middle regions (except January and February). In the lower regions water

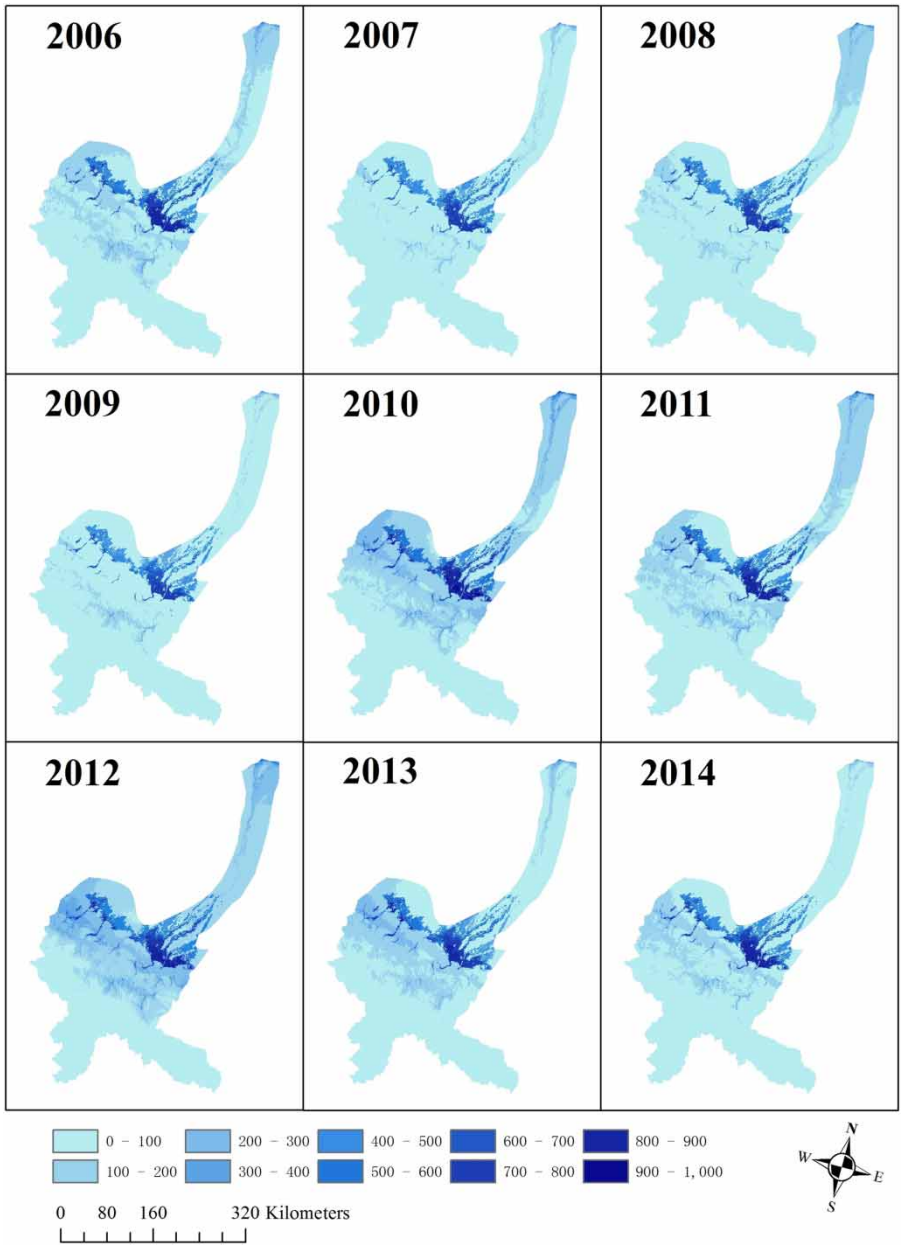

Figure 6 | Spatial distribution of annual ET_a rates during 2006–2014 in the HRB (all in mm yr^{-1}).

deficits occurred during May to September. From October to April, water budget was a basic equilibrium, because the river was drying up during these months. Additionally, the annual deficit was estimated to be 100 mm in the middle regions and 44 mm in the lower regions. Furthermore, the amount of available water was sufficient to satisfy ET_a in most months in the upper regions, where the mean annual water surplus was 150 mm.

DISCUSSION

There is great debate regarding whether proportionality parameter b is constant. Huntington *et al.* (2011) applied a modified AA model with $b = 1$ to estimate monthly and annual ET_a from arid shrublands of the southwestern USA and obtained quite satisfactory prediction accuracy. Ma *et al.* (2015b) applied a modified CR-based AA model to

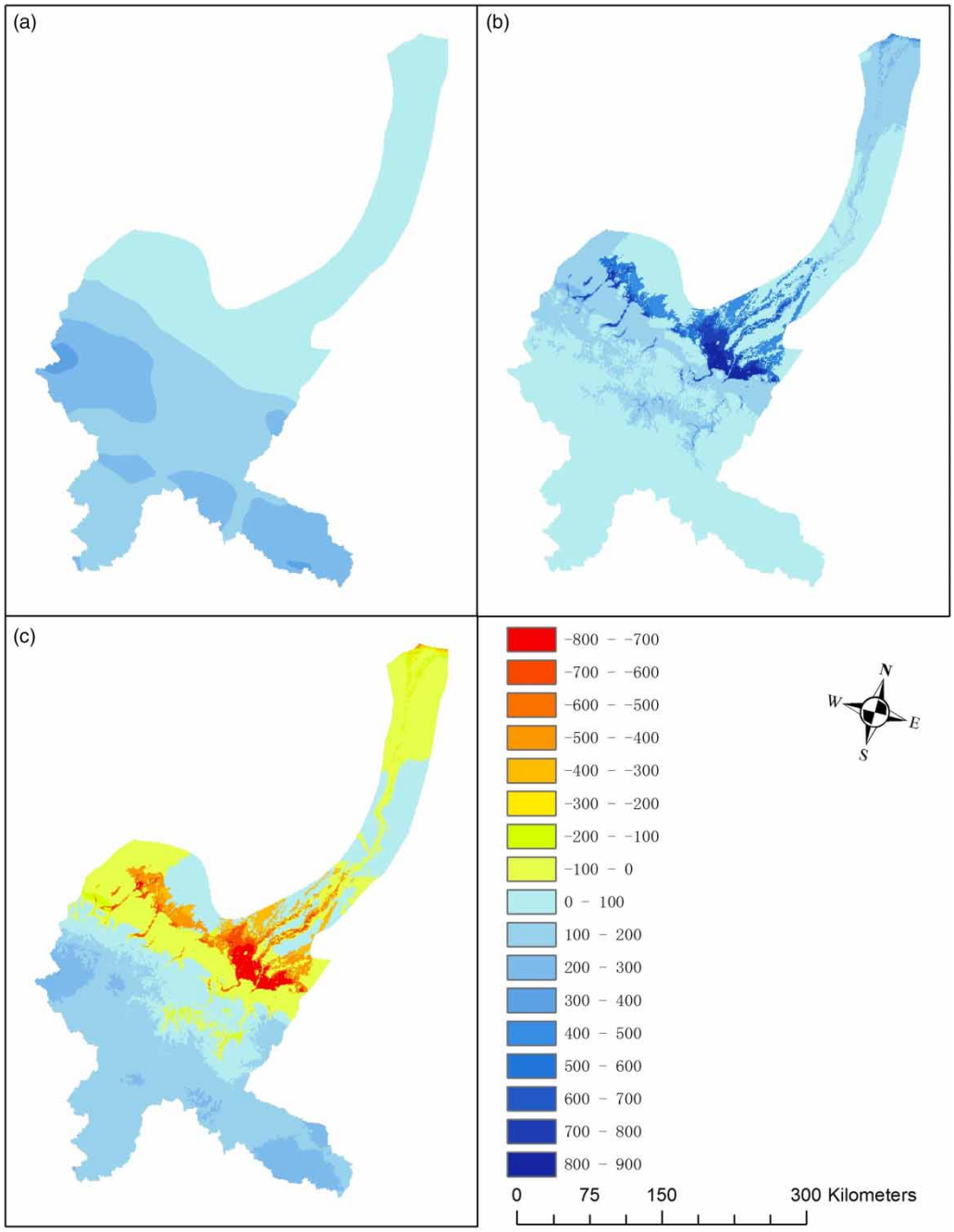

Figure 7 | Spatial distribution of mean annual (a) precipitation (P), (b) ET_a, and (c) $P - ET_a$ difference during 2006–2014 in the HRB (all in mm yr^{-1}).

obtain daily ET_a in the alpine steppe of the Tibetan Plateau and believed that a symmetric CR ($b = 1$) contradicted previous research that used default parameter values to claim an asymmetric CR in arid and semiarid regions of the Tibetan Plateau. Sugita *et al.* (2001) demonstrated that b equals unity only when the underlying surface is smooth enough and soil moisture is sufficient. Furthermore, Ma *et al.* (2015b) suggested that a strictly symmetric CR is difficult to achieve because the actual wet surface is too small or too large, or there is the influence of some additional heat

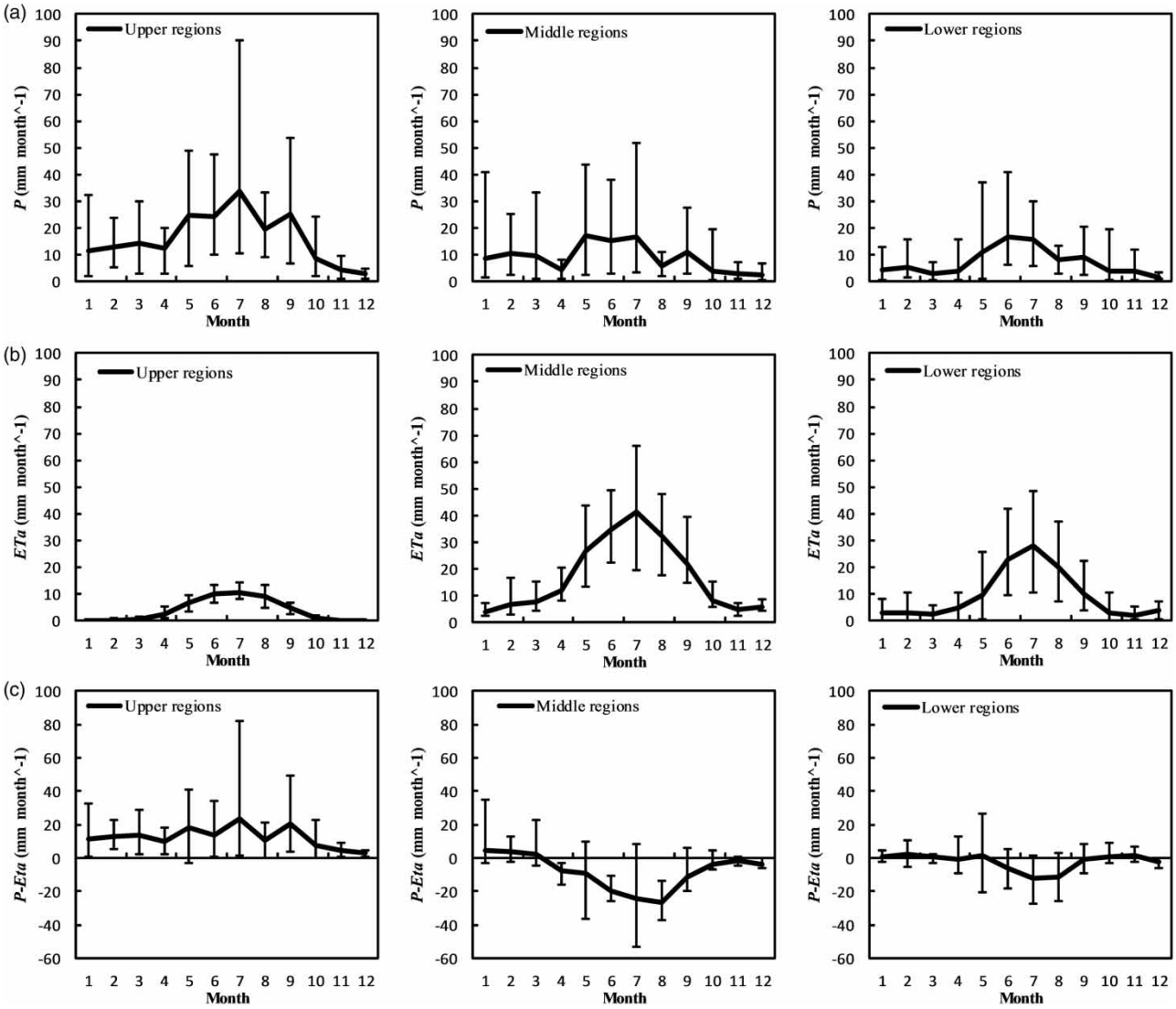

Figure 8 | Monthly mean (a) precipitation (P), (b) ET_a, and (c) $P - ET_a$ difference from 2006 to 2014 in the upper, middle, and lower regions. The bars indicate the maximum and minimum values of P, ET_a, and $P - ET_a$ difference for the land cover types.

transfer though the bottom or side of pans. Kahler & Brutsaert (2006) also suggested that the asymmetry with ET_p given by pan evaporation was due to the effect of a significant bottom or sidewall effect of pans. However, Szilagyi (2007) and Brutsaert (2015) demonstrated that the asymmetry is the inherent nature rather than the cases. In the present study, Equation (14), proposed by Crago *et al.* (2016), was used to estimate the ET_a. The present CR model is a self-adjusting CR since b could be obtained for each daily and each grid value as $b = (1 - x_{min})/x_{min}$ (Crago *et al.* 2016). The CR is only linear (symmetric) when $x_{min} = 0.5$. The definition of variable X defined by Crago *et al.* (2016) is essentially the same as the definition of Szilagyi *et al.* (2017). However, the relationship between y and x or X is actually still unspecified. Brutsaert (2015) and Crago *et al.* (2016) recommended the simple polynomial to add some flexibility in CR formulations, so that its parameters can be calibrated easily. Hence, Equation (16) was adopted in this study.

Two definitions of ET_{pmax} reported by Crago *et al.* (2016) and Szilagyi *et al.* (2017) were contrasted above to select an appropriate definition according to conditions in

the study basin. The ET_{pmax} defined by Szilagyi *et al.* (2017) was chosen because of the physically based limits, i.e., $ET_w \le ET_p \le ET_{p\max}$. We found that $ET_p - ET_{pds} > 0$ where the elevation is more than approximately 2,300 m asl (not displayed). Because $T_{ws} \approx T_a$ in the mountainous regions, one obtains the following:

$$ET_p - ET_{pds} = \frac{\Delta}{\Delta+\gamma}\left(\frac{R_n - G}{\lambda} - f(U)e_s\right) - \frac{\Delta}{\Delta+\gamma}f(U)e_a. \tag{18}$$

ET_{pds} defined by Crago *et al.* (2016) is not applicable where $ET_p - ET_{pds} > 0$, i.e., $((R_n - G)/(\lambda)) - f(U)\ e_s > (\gamma/\Delta)f(U)e_a$. In the present study, ET_{pds} was unsuitable in the mountainous regions. Applicability of ET_{pds} depends on the combined effect of R_n, wind speed, T_a, and elevation. Ma & Zhang (2017) thought that the reason of inapplicability of ET_{pds} is mainly due to small wind speed and large available energy. This conclusion is essentially consistent with comments of Ma & Zhang (2017) since the comments had assumed time-invariant T_{ws} and landscape in setting the numerical experiment. Although the values of the wind speed in the mountainous regions are higher than these values in the plains regions, as shown in Figure 3, the available energy and roughness length should play roles in impacting the relationship between ET_p and ET_{pds} as well. That is, when ET_{pds} is defined, wind speed is not the only factor that needs to be considered.

In the current study, the HRB was divided into two terrain conditions: the plains regions (below 2,000 m asl) and the mountainous regions (above 2,000 m asl), while the HRB was divided into two underlying surface conditions: vegetated regions and unvegetated regions. Hence, to precisely describe the spatial distribution of ET_a, the σ of each condition was recalculated according to the regional water balance and the basic evaporation laws, as mentioned above (Table 1). The underlying surface of the mountainous regions changed with elevation; therefore, a linear function of elevation was used to illustrate the change of σ in the mountainous regions. Note that calibrate σ varies significantly. This may show that this CR method might not be used in extreme cold and arid areas.

Obviously, estimated ET_a has some uncertainties. For example, extreme cold and arid areas often have precipitation saved in the form of snow and ice until they melt in subsequent years. This means that ΔW has a greater effect at smaller time scales, but this should not be assumed to be 0. However, in the present study, it had to be assumed to be 0, as explained above. Moreover, over the past few years, the data obtained from the Gravity Recovery and Climate Experiment (GRACE) have notably improved our understanding of water storage change at monthly time scales in large basins globally (Scanlon *et al.* 2015; Save *et al.* 2016). However, the area of the HRB makes it unsuitable for analysis because it uses GRACE data. Secondly, there are uncertainties regarding the function relations of σ and elevation in the mountainous regions. A linear function was selected since it was easy to understand and be calibrated; however, this does not mean that linear function is the best relationship between σ and elevation. In addition, the values of α changed with elevation rather than time. The values of α were also reported to be a function of surface meteorological and environmental factors (Aminzadeh & Or 2014). Obviously, the setting of values of α can make a significant difference in the calibration parameter σ. As noted by Szilagyi *et al.* (2017), any CR-based method is quite sensitive to the parameter value of α. Finally, the reanalysis dataset and runoff data still had significant uncertainties in extreme cold and arid areas because of the extremely sparse meteorological stations and harsh natural conditions. Although ET_a estimated in the mountainous regions remains uncertain and could not be verified at daily and monthly time scales, this study not only provides a new concept for calibration, but also a potential solution for different underlying surfaces and time scales.

CONCLUSIONS

In this study, we used the generalized CR to estimate ET_a rates during 2006–2014 at daily time scales in extreme cold and arid areas. The HRB served as a prime example. The China Meteorological Forcing Dataset and MODIS data were used to calculate CR components and to analyze regional water balance. Comparison and analysis revealed that correction of the wind function had more significant effects than correction of T_w. $ET_{p\max}$, defined by Crago *et al.* (2016), was not applicable in the study basin, especially in the

mountainous regions. Hence, we adopted $ET_{p\max}$, defined by Szilagyi *et al.* (2017). Since available data in the HRB were limited, the validity and accuracy of the calculated ET_a were verified using a regional water balance method at annual time scales. The coefficient σ was calibrated based on the elevation and underlying surface types. Mean annual ET_a estimated using optimal values of σ matched the mean annual ET_{wb} well, while there was deviation between annual ET_a and annual ET_{wb}. Based on the model estimations, spatial and temporal distributions of ET_a and the water budget in the basin from 2006 to 2014 could offer a reference at monthly or even daily time scales. The mean annual ET_a ranged from 2.3 mm to 800 mm during 2006–2014. ET_a rates in the plains regions were higher than those in the mountainous regions, with the highest values being observed in croplands and shrublands along the riverside. Most of ET_a was concentrated in the months of May to September, accounting for 89% of the mean annual ET_a (42 mm) in the upper regions, 76% (159 mm) in the middle regions, and 80% (105 mm) in the lower regions. A water deficit occurred in the middle and lower regions, and a water surplus occurred in the upper regions. The annual deficit was estimated to be 100 mm in the middle regions and 44 mm in the lower regions. The amount of available water was sufficient to satisfy ET_a in most months in the upper regions, where the mean annual water surplus was 150 mm.

If meteorological stations and *in situ* flux stations could be established in the mountainous and desert regions in the future, the accuracy of estimated ET_a and water management efficiency could be improved. Moreover, a model-independent calculation of α considering underlying surface conditions and environmental conditions has important implications for a calibration-free CR model. That CR model could be easily applied to all kinds of conditions, including extreme cold and arid areas. However, additional studies should be conducted to further improve the model.

ACKNOWLEDGEMENTS

The forcing datasets used in this study were developed by the Data Assimilation and Modeling Center for Tibetan Multi-spheres, Institute of Tibetan Plateau Research, and Chinese Academy of Sciences (http://westdc.westgis.ac.cn/data/). MODIS data and DEM data were provided by the Geospatial Data Cloud site, Computer Network Information Center, and Chinese Academy of Sciences (http://www.gscloud.cn). This work was supported by the National Natural Science Foundation of China (51509202 and 51679185). We thank LetPub (www.letpub.com) for its linguistic assistance during the preparation of this manuscript. We are grateful to the four anonymous reviewers and the editor whose valuable comments and suggestions led to important revisions.

REFERENCES

Allen, R. G., Pereira, L. S., Raes, D. & Smith, M. 1998 *Crop Evapotranspiration-Guidelines for Computing Crop Water Requirements.* FAO Irrigation and Drainage Paper 56. Food and Agriculture Organization of the United Nations, Rome, 300, 6541.

Aminzadeh, M. & Or, D. 2014 Energy partitioning dynamics of drying terrestrial surfaces. *Journal of Hydrology* **519**, 1257–1270.

Aminzadeh, M. & Or, D. 2017 The complementary relationship between actual and potential evaporation for spatially heterogeneous surfaces. *Water Resources Research* **53** (1), 580–601.

Aminzadeh, M., Roderick, M. L. & Or, D. 2016 A generalized complementary relationship between actual and potential evaporation defined by a reference surface temperature. *Water Resources Research* **52** (1), 385–406.

Bastiaanssen, W. G. M., Menenti, M., Feddes, R. A. & Holtslag, A. A. M. 1998 A remote sensing surface energy balance algorithm for land (SEBAL): 1. *Formulation. Journal of Hydrology* **212**, 198–212.

Bisht, G., Venturini, V., Islam, S. & Jiang, L. 2005 Estimation of the net radiation using MODIS (Moderate resolution imaging spectroradiometer) data for clear sky days. *Remote Sensing of Environment* **97** (1), 52–67.

Bouchet, R. J. 1963 Evapotranspiration réelle et potentielle, signification climatique (Real and potential evapotranspiration climate meaning). *IASH Publication* **62**, 134–142.

Brutsaert, W. 1982 *Evaporation Into the Atmosphere: Theory, History, and Applications.* Springer, New York, USA, pp. 299.

Brutsaert, W. 2005 *Hydrology: An Introduction.* Cambridge University Press, New York, USA, pp. 605.

Brutsaert, W. 2015 A generalized complementary principle with physical constraints for land-surface evaporation. *Water Resources Research* **51** (10), 8087–8093.

Brutsaert, W. & Parlange, M. B. 1998 Hydrologic cycle explains the evaporation paradox. *Nature* **396** (5), 300.

Brutsaert, W. & Stricker, H. 1979 An advection-aridity approach to estimate actual regional evapotranspiration. *Water Resources Research* **15** (2), 443–450.

Cleugh, H. A., Leuning, R., Mu, Q. & Running, S. W. 2007 Regional evaporation estimates from flux tower and MODIS satellite data. *Remote Sensing of Environment* **106** (3), 285–304.

Crago, R. & Qualls, R. 2013 The value of intuitive concepts in evaporation research. *Water Resources Research* **49** (9), 6100–6104.

Crago, R. D., Qualls, R. J. & Feller, M. 2010 A calibrated advection-aridity evaporation model requiring no humidity data. *Water Resources Research* **46** (9), W09519. doi: 10.1029/2009WR008497.

Crago, R., Szilagyi, J., Qualls, R. & Huntington, J. 2016 Rescaling the complementary relationship for land surface evaporation. *Water Resources Research* **52** (11), 8461–8471.

Eichinger, W. E., Parlange, M. B. & Stricker, H. 1996 On the concept of equilibrium evaporation and the value of the Priestley-Taylor coefficient. *Water Resources Research* **32** (1), 161–164.

Gao, G., Xu, C. Y., Chen, D. & Singh, V. P. 2012 Spatial and temporal characteristics of actual evapotranspiration over Haihe River basin in China. *Stochastic Environmental Research and Risk Assessment* **26** (5), 655–669.

Glenn, E. P., Huete, A. R., Nagler, P. L., Hirschboeck, K. K. & Brown, P. 2007 Integrating remote sensing and ground methods to estimate evapotranspiration. *Critical Reviews in Plant Sciences* **26** (3), 139–168.

Granger, R. J. & Gray, D. M. 1989 Evaporation from natural nonsaturated surfaces. *Journal of Hydrology* **111**, 21–29.

Guo, Y. & Shen, Y. J. 2015 Quantifying water and energy budgets and the impacts of climatic and human factors in the Haihe River Basin, China: 1. Model and validation. *Journal of Hydrology* **528**, 206–216.

Han, S., Hu, H. & Tian, F. 2012 A nonlinear function approach for the normalized complementary relationship evaporation model. *Hydrological Processes* **26** (26), 3973–3981.

Han, S., Tian, F. & Hu, H. 2014 Positive or negative correlation between actual and potential evaporation? Evaluating using a nonlinear complementary relationship model. *Water Resources Research* **50** (2), 1322–1336.

Haverd, V., Cuntz, M., Griffith, D., Keitel, C., Tadros, C. & Twining, J. 2011 Measured deuterium in water vapour concentration does not improve the constraint on the partitioning of evapotranspiration in a tall forest canopy, as estimated using a soil vegetation atmosphere transfer model. *Agricultural and Forest Meteorology* **151** (6), 645–654.

He, J. & Yang, K. 2011 *China Meteorological Forcing Dataset*. Cold and Arid Regions Science Data Center at Lanzhou, China.

Hobbins, M. T., Ramirez, J. A. & Brown, T. C. 2001 The complementary relationship in estimation of regional evapotranspiration: an enhanced advection-aridity model. *Water Resources Research* **37** (5), 1389–1403.

Hobbins, M. T., Wood, A., McEvoy, D. J., Huntington, J. L., Morton, C., Anderson, M. & Hain, C. 2016 The evaporative demand drought index. Part I: linking drought evolution to variations in evaporative demand. *Journal of Hydrometeorology* **17** (6), 1745–1761.

Huntington, J. L., Szilagyi, J., Tyler, S. W. & Pohll, G. M. 2011 Evaluating the complementary relationship for estimating evapotranspiration from arid shrublands. *Water Resources Research* **47** (5), W05533. doi: 10.1029/2010wr009874.

Jaksa, W. T., Sridhar, V., Huntington, L. & Khanal, M. 2013 Evaluation of the complementary relationship using Noah land surface model and North American Regional Reanalysis (NARR) data to estimate evapotranspiration in semiarid ecosystems. *Journal of Hydrometeorology* **14** (1), 345–359.

Kahler, D. M. & Brutsaert, W. 2006 Complementary relationship between daily evaporation in the environment and pan evaporation. *Water Resources Research* **42** (5), W05413. doi: 10.1029/2005wr004541.

Lavers, D. A., Villarini, G., Allen, R. P., Wood, E. F. & Wade, A. J. 2012 The detection of atmospheric rivers in atmospheric reanalyses and their links to British winter floods and the large-scale climatic circulation. *Journal of Geophysical Research: Atmospheres* **117**, D20106 doi: 10.1029/2012JD018027.

Liu, S., Bai, J., Zhou, H., Jia, L. & Lu, L. 2009 Estimation of evapotranspiration in the Mu Us Sandland of China. *Hydrology and Earth System Sciences Discussions* **6** (5), 5977–6006.

Lyu, J., Shen, B. & Li, H. 2015 Dynamics of major hydro-climatic variables in the headwater catchment of the Tarim River Basin, Xinjiang, China. *Quaternary International* **380**, 143–148.

Ma, N. & Zhang, Y. 2017 Comment on 'Rescaling the complementary relationship for land surface evaporation' by R. Crago *et al*. *Water Resources Research* **53** (7), 6340–6342.

Ma, N., Wang, N., Zhao, L., Zhang, Z., Dong, C. & Shen, S. 2014 Observation of mega-dune evaporation after various rain events in the hinterland of Badain Jaran Desert, China. *Chinese Science Bulletin* **59** (2), 162–170.

Ma, N., Zhang, Y., Xu, C.-Y. & Szilagyi, J. 2015a Modeling actual evapotranspiration with routine meteorological variables in the data-scarce region of the Tibetan Plateau: comparisons and implications. *Journal of Geophysical Research: Biogeosciences* **120** (8), 1638–1657.

Ma, N., Zhang, Y., Szilagyi, J., Guo, Y., Zhai, J. & Gao, H. 2015b Evaluating the complementary relationship of evapotranspiration in the alpine steppe of the Tibetan Plateau. *Water Resources Research* **51** (2), 1069–1083.

Mallick, K., Boegh, E., Trebs, I., Alfieri, J. G., Kustas, W. P., Prueger, J. H., Niyogi, D., Das, N., Drewry, D. T., Hoffmann, L. & Jarvis, A. J. 2015 Reintroducing radiometric surface temperature into the Penman-Monteith formulation. *Water Resources Research* **51** (8), 6214–6243.

Mariotto, I., Gutschick, V. P. & Clason, D. L. 2011 Mapping evapotranspiration from ASTER data through GIS spatial integration of vegetation and terrain features. *Photogrammetric Engineering & Remote Sensing* **77** (5), 483–493.

McEvoy, D. J., Huntington, J. L., Hobbins, M. T., Wood, A., Morton, C., Anderson, M. & Hain, C. 2016 The evaporative demand drought index. Part II: CONUS-wide assessment against common drought indicators. *Journal of Hydrometeorology* **17** (6), 1763–1779.

Mesinger, F., DiMego, G., Kalnay, E., Mitchell, K., Shafran, P. C., Ebisuzaki, W., Jović, D., Woollen, J., Rogers, E., Berbery, E. H., Ek, M. B., Fan, Y., Grumbine, R., Higgins, W., Li, H., Lin, Y., Manikin, G., Parrish, D. & Shi, W. 2006 North American regional reanalysis. *Bulletin of the American Meteorological Society* **87** (3), 343–360.

Monteith, J. L. 1965 Evaporation and environment. *Symposia of the Society for Experimental Biology* **19**, 205–234.

Monteith, J. L. & Unsworth, M. H. 2013 *Principles of Environmental Physics: Plant, Animals, and the Atmosphere.* Academic Press, Oxford, UK.

Morton, F. I. 1983 Operational estimates of areal evapotranspiration and their significance to the science and practice of hydrology. *Journal of Hydrology* **66** (1–4), 1–76.

Oki, T. & Kanae, S. 2006 Global hydrological cycles and world water resources. *Science* **313** (5790), 1068–1072.

Penman, H. L. 1948 Natural evaporation from open water, bare soil and grass. *Proceedings of the Royal Society of London. Series A, Mathematical and Physical Sciences* **193** (1032), 120–145.

Priestley, C. H. B. & Taylor, R. J. 1972 On the assessment of surface heat flux and evaporation using large-scale parameters. *Monthly Weather Review* **100** (2), 81–92.

Qualls, R. J. & Gultekin, H. 1997 Influence of components of the advection-aridity approach on evapotranspiration estimation. *Journal of Hydrology* **199** (1), 3–12.

Ryu, Y., Baldocchi, D. D., Ma, S. & Hehn, T. 2008 Interannual variability of evapotranspiration and energy exchange over an annual grassland in California. *Journal of Geophysical Research* **113**, D09104. doi: 10.1029/2007jd009263.

Save, H., Bettadpur, S. & Tapley, B. D. 2016 High resolution CSR GRACE RL05 mascons. *Journal of Geophysical Research: Solid Earth* **121** (10), 7547–7569.

Scanlon, B. R., Zhang, Z., Reedy, R. C., Pool, D. R., Save, H., Long, D., Chen, J., Woloch, D. M., Conway, B. D. & Winester, D. 2015 Hydrologic implications of GRACE satellite data in the Colorado River Basin. *Water Resources Research* **51** (12), 9891–9903.

Singh, R. K., Irmak, A., Irmak, S. & Martin, D. L. 2008 Application of SEBAL model for mapping evapotranspiration and estimating surface energy fluxes in south-central Nebraska. *Journal of Irrigation and Drainage Engineering* **134** (3), 273–285.

Su, Z. 2002 The Surface Energy Balance System (SEBS) for estimation of turbulent heat fluxes. *Hydrology and Earth System Sciences* **6** (1), 85–99.

Sugita, M., Usui, J., Tamagawa, I. & Kaihotsu, I. 2001 Complementary relationship with a convective boundary layer model to estimate regional evaporation. *Water Resources Research* **37** (2), 353–365.

Szilagyi, J. 2007 On the inherent asymmetric nature of the complementary relationship of evaporation. *Geophysical Research Letters* **34** (2), 155–164.

Szilagyi, J. 2014 Temperature corrections in the Priestley-Taylor equation of evaporation. *Journal of Hydrology* **519**, 455–464.

Szilagyi, J. 2015 Complementary-relationship-based 30 year normals (1981–2010) of monthly latent heat fluxes across the contiguous United States. *Water Resources Research* **51** (11), 9367–9377.

Szilagyi, J. & Jozsa, J. 2008 New findings about the complementary relationship-based evaporation estimation methods. *Journal of Hydrology* **354** (1), 171–186.

Szilagyi, J., Crago, R. & Qualls, R. J. 2016 Testing the generalized complementary relationship of evaporation with continental-scale long-term water-balance data. *Journal of Hydrology* **540**, 914–922.

Szilagyi, J., Crago, R. & Qualls, R. 2017 A calibration-free formulation of the complementary relationship of evaporation for continental-scale hydrology. *Journal of Geophysical Research: Atmospheres* **122** (1), 264–278.

Vinukollu, R. K., Wood, E. F., Ferguson, C. R. & Fisher, J. B. 2011 Global estimates of evapotranspiration for climate studies using multi-sensor remote sensing data: evaluation of three process-based approaches. *Remote Sensing of Environment* **115** (3), 801–823.

Wang, K. & Dickinson, R. E. 2012 A review of global terrestrial evapotranspiration: observation, modeling, climatology, and climatic variability. *Reviews of Geophysics* **50** (2), RG2005. doi: 10.1029/2011rg000373.

Wang, J., Bastiaanssen, W. G., Ma, Y. & Pelgrum, H. 1988 Aggregation of land surface parameters in the oasis-desert systems of north-west China. *Hydrological Processes* **12**, 2133–2147.

Wang, Y., Liu, B., Su, B., Zhai, J. & Gemmer, M. 2011 Trends of calculated and simulated actual evaporation in the Yangtze River basin. *Journal of Climate* **24** (16), 4494–4507.

Xu, C. Y. & Singh, V. P. 2005 Evaluation of three complementary relationship evapotranspiration models by water balance approach to estimate actual regional evapotranspiration in different climatic regions. *Journal of Hydrology* **308** (1), 105–121.

Yang, H., Yang, D., Lei, Z., Sun, F. & Cong, Z. 2008 Regional variability of the complementary relationship between actual and potential evapotranspiration. *Journal of Tsinghua University (Science and Technology)* **48**, 1413–1416 (in Chinese).

Yang, K., He, J., Tang, W., Qin, J. & Cheng, C. C. K. 2010 On downward shortwave and longwave radiations over high altitude regions: observation and modeling in the Tibetan Plateau. *Agricultural and Forest Meteorology* **150** (1), 38–46.

Yang, H., Yang, D. & Lei, Z. 2013 Seasonal variability of the complementary relationship in the Asian monsoon region. *Hydrological Processes* **27** (19), 2736–2741.

Zhao, C., Shen, B., Huang, L., Lei, Z., Hu, H. & Yang, S. 2009 A dissipative hrdrological model for the Hotan Oasis (DHMHO). *Water Resources Management* **23** (6), 1183–1210.

Zheng, J., Bian, J., Ge, Q., Hao, Z., Yin, Y. & Liao, Y. 2013 The climate regionalization in China for 1981–2010. *Chinese Science Bulletin* **58** (30), 3088–3099 (in Chinese).

First received 1 June 2017; accepted in revised form 16 October 2017. Available online 20 November 2017